CHEMISTRY OF MATERIALS
Article

Chem. Mater. **2010,** *22,* 3369–3382 3369
DOI:10.1021/cm903848h

Structure and Properties of $Sr_{1-x}Ca_xMn_{0.5}Ru_{0.5}O_3$ Perovskites: Using Chemical Pressure to Control Mn/Ru Mixed Valency

Rebecca A. Ricciardo,[†] Heather L. Cuthbert,[†] Patrick M. Woodward,*[,†] Qingdi Zhou,[‡] Brendan J. Kennedy,*[,‡] Zhaoming Zhang,[§] Maxim Avdeev,[⊥] and Ling-Yun Jang[#]

[†]*Department of Chemistry, The Ohio State University, 100 West 18th Avenue, Columbus, Ohio 43210-1185,* [‡]*School of Chemistry, The University of Sydney, Sydney, New South Wales 2006, Australia,* [§]*Institute of Materials Engineering, ANSTO, Private Mail Bag 1, Menai, New South Wales, 2234, Australia,* [⊥]*Bragg Institute, ANSTO, Private Mail Bag 1, Menai, New South Wales, 2234, Australia, and* [#]*Research Division, National Synchrotron Radiation Research Center, Hsinchu 30076, Taiwan*

Received December 24, 2009. Revised Manuscript Received March 28, 2010

The structure and properties of $Sr_{1-x}Ca_xRu_{0.5}Mn_{0.5}O_3$ compositions have been investigated. Both bond distances and X-ray absorption measurements reveal $Mn^{3+} + Ru^{5+} \leftrightarrow Mn^{4+} + Ru^{4+}$ mixed valency across the entire series. Despite a complete lack of Ru/Mn chemical order, all samples magnetically order between 220 and 300 K. The characteristics and type of magnetic order are sensitive to the occupation and ordering of the Mn e_g orbitals, which can be manipulated by changes in chemical pressure, via the Sr/Ca ratio. Sr-rich samples are tetragonally distorted by a cooperative Jahn−Teller distortion (CJTD) that leads to an elongation of the *c*-axis as well as antiphase rotations of the octahedra about the *c*-axis ($a^0a^0c^-$ tilt system). The CJTD results from orbital ordering involving occupied d_{z^2} orbitals on Mn^{3+}, which stabilize C-type antiferromagnetic order. For Sr-rich samples, the various oxidation states contribute in approximately equal proportions (i.e., $Ru^{+4.5}$ and $Mn^{+3.5}$). Substituting Ca^{2+} for Sr^{2+} triggers additional rotations of the octahedra ($a^-b^+a^-$ tilt system) that result in orthorhombic symmetry for $Sr_{1-x}Ca_xMn_{0.5}Ru_{0.5}O_3$ samples with $x \geq 0.3$. The crossover to orthorhombic symmetry is accompanied by the loss of orbital order and the emergence of an itinerant electron ferrimagnetic state. X-ray absorption near edge structure (XANES) measurements show that as the Ca^{2+} content increases there is a shift in the valence degeneracy toward $Mn^{4+} + Ru^{4+}$. This helps to explain the absence of orbital ordering in Ca-rich samples, as well as the crossover from antiferromagnetism to ferrimagnetism. Neutron diffraction and ac susceptibility measurements show that $CaRu_{0.5}Mn_{0.5}O_3$ undergoes magnetic phase separation into a disordered ferrimagnetic state ($T_C \approx 230$ K) and a G-type antiferromagnetic state ($T_N \approx 95$ K).

1. Introduction

ABO_3 perovskites containing either manganese or ruthenium are among the most interesting and heavily studied perovskites. Behavior ranging from itinerant electron ferromagnetism to localized electron antiferromagnetism can be realized (Figure 1). The properties are not only sensitive to the identity of the B-site cation, they can also be manipulated by changing the size and/or charge of the A-site cation.

$SrMnO_3$ and $CaMnO_3$ contain Mn^{4+} with a $t_{2g}^3e_g^0$ electron configuration. The presence of half-filled t_{2g} and empty e_g orbitals results in antiferromagnetic Mott insulating behavior in both cases, with Néel temperatures of ∼235 K (Sr) and ∼120 K (Ca).[1] Antiferromagnetic superexchange coupling to all six neighbors leads to the G-type antiferromagnetic structure in both instances. $LaMnO_3$ is an orbitally ordered, antiferromagnetic insulator ($T_N \approx 140$ K).[2] The high-spin Mn^{3+} ion has a $t_{2g}^3e_g^1$ electron configuration that is responsible for local Jahn−Teller distortions of the octahedra. The preferential occupation of alternating Mn $3d_{3x^2-r^2}$ and Mn $3d_{3z^2-r^2}$ orbitals results in a cooperative Jahn−Teller distortion that drives an expansion of the unit cell in two directions and contraction in the third direction. This pattern of orbital ordering is directly responsible for stabilizing the A-type antiferromagnetic structure. Substituting a divalent alkaline earth ion, such as Ca^{2+}, for La^{3+} raises the average Mn oxidation state eventually leading to delocalization of the Mn e_g electrons and double exchange mediated ferromagnetic metallic behavior. Further substitution of divalent alkaline earth ions leads to more complex patterns of orbital and magnetic order.[3]

$SrRuO_3$ is a metallic ferromagnet with a $T_C = 165$ K. The saturation moment, $M_s = 1.10\,\mu_B$ per Ru, is smaller than the expected spin only value (∼2 μ_B) for a low spin Ru^{4+} ion with a $t_{2g}^4e_g^0$ electron configuration. In the $Sr_{1-x}Ca_xRuO_3$ series substitution of Ca^{2+} for Sr^{2+} narrows the π^* conduction band. Although metallic conductivity is retained for all levels of calcium substitution, the T_C decreases

*Corresponding author.

(1) Chmaissem, O.; Dabrowski, B.; Kolesnik, S.; Mais, J.; Brown, D. E.; Kruk, R.; Prior, P.; Pyles, B.; Jorgensen, J. D. *Phys. Rev. B* **2001**, *64*, 134412.
(2) Sakai, N.; Fjellvag, H.; Lebech, B. *Acta Chem. Scand.* **1997**, *51*, 904.
(3) Schiffer, P.; Ramirez, A. P.; Bao, W.; Cheong, S.-W. *Phys. Rev. Lett.* **1995**, *75*, 3336.

Published on Web 05/10/2010

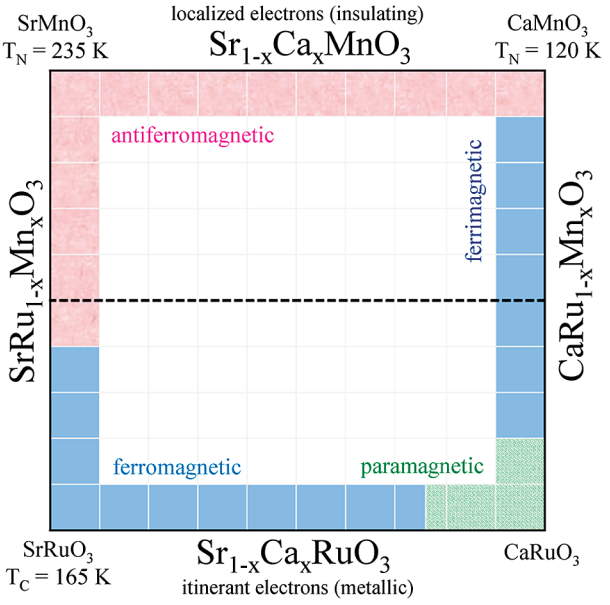

Figure 1. Magnetic and electrical behavior of $CaRuO_3$, $SrRuO_3$, $CaMnO_3$, and $SrMnO_3$ (the metastable cubic perovskite form) and their solid solutions. The dashed line represents the $Sr_{1-x}Ca_xMn_{0.5}Ru_{0.5}O_3$ solid solution.

monotonically, eventually giving way to paramagnetic behavior for Ca-rich samples ($x > 0.8$).[4] The calcium substitution not only leads to a decrease in T_C, it decreases the ferromagnetic volume fraction of the sample, resulting in a magnetically inhomogeneous phase known as a Griffith's phase [5,6].

The rich behavior of the manganite and ruthenate perovskites provides a compelling motivation to study the mixed $ARu_{1-x}Mn_xO_3$ perovskites. In both $CaRu_{1-x}Mn_xO_3$ and $SrRu_{1-x}Mn_xO_3$ systems, the conductivity steadily decreases as Mn is substituted for Ru.[7,8] In $SrRu_{1-x}Mn_xO_3$,T_C also decreases as manganese substitutes for ruthenium, crossing over from metallic ferromagnetism to semiconducting antiferromagnetism for $x \geq 0.4$.[8,9] Over the range $0.4 \leq x \leq 0.94$, orbital ordering results in a tetragonally distorted unit cell and C-type antiferromagnetic order.[9−11] These observations imply the presence of Jahn−Teller distortions of octahedra containing Mn^{3+}. Variable-temperature X-ray diffraction studies of $SrRu_{0.5}Mn_{0.5}O_3$ show that the cooperative Jahn−Teller distortion (and hence the orbital order) disappears above ~523 K.[12]

The $CaRu_{1-x}Mn_xO_3$ system has been extensively studied. Paramagnetic $CaRuO_3$ quickly becomes ferromagnetic ($x \geq 0.2$) as manganese is introduced.[13,14] T_C climbs to a maximum of 210−220 K near $x = 0.7$.[14] The lack of Ru/Mn order makes the ferromagnetic state unusual in several regards. Neutron diffraction studies of both $CaRu_{0.6}Mn_{0.4}O_3$[13] and $CaRu_{0.4}Mn_{0.6}O_3$[15] reveal the coexistence of antiferromagnetically ordered and ferromagnetically ordered regions. Both X-ray magnetic circular dichroism (XMCD)[16] and magnetic Compton scattering[14,17] on samples spanning the $CaRu_{1-x}Mn_xO_3$ series reveal that the Mn and Ru moments are oriented antiparallel to each other. Thus the ferromagnetic state is more accurately described as a (disordered) ferrimagnetic state. This finding explains why the saturation moment is always much smaller (~1 μ_B per transition metal ion) than expected for true ferromagnetism. Neutron diffraction studies do not reveal the ferrimagnetic nature of the samples due to the Mn/Ru disorder.

The origin of ferrimagnetism in the $CaRu_{1-x}Mn_xO_3$ system is not universally agreed upon. In Mn-rich samples the introduction of ruthenium leads to electron transfer that converts some of the Mn^{4+} into Mn^{3+} creating Ru^{5+} in the process. Shames et al. attribute ferromagnetism in part to Mn^{3+}−O−Mn^{4+} double exchange interactions, as well as ferromagnetic Mn^{3+}−O−Ru superexchange interactions [15]. Taniguchi et al. also invoke ferromagnetic Mn^{3+}−O−Mn^{4+} coupling, but assume antiferromagnetic coupling between Ru^{5+} and Mn.[14] Kawanaka et al. argue that ferromagnetism in Ru-rich samples can be explained by spin fluctuation theory based on itinerant electron magnetism as in $SrRuO_3$, rather than double exchange ferromagnetism.[13] Terai et al. propose that delocalization of Ru t_{2g} electrons within a matrix of antiparallel, localized Mn t_{2g} spins is responsible for the ferrimagnetic ordering, much as it is in Sr_2FeMoO_6 and Sr_2CrReO_6 (so-called double perovskite-double exchange).[16]

Although the edges of the $Sr_{1-x}Ca_xRu_{1-y}Mn_yO_3$ pseudophase diagram shown in Figure 1 have been extensively studied, the middle regions have not. In this study, the evolution from $SrRu_{0.5}Mn_{0.5}O_3$ to $CaRu_{0.5}Mn_{0.5}O_3$ (marked by the dashed line in Figure 1) is investigated. $SrRu_{0.5}Mn_{0.5}O_3$ is a tetragonal, C-type antiferromagnet ($T_N \approx 230$ K) that exhibits orbital ordering and activated (variable range hopping) conductivity.[8−12] $CaRu_{0.5}Mn_{0.5}O_3$ is an orthorhombic, ferrimagnet ($T_c \approx 210$ K) that does not show obvious signs of orbital order. Its room temperature conductivity is on the order of 50 S cm^{-1} and nearly temperature-independent.[13,14,16,17]

(4) Cao, G.; McCall, S.; Shepard, M.; Crow, J. E.; Guertin, R. P. *Phys. Rev. B* **1997**, *56*, 321.
(5) Jin, C.-Q.; Zhou, J.-S.; Goodenough, J. B.; Liu, Q. Q.; Zhao, J. G.; Yang, L. X.; Yu, Y.; Yu, R. C.; Katsura, T.; Shatskiy, A.; Ito, E. *Proc. Natl. Acad. Sci. U.S.A.* **2008**, *105*, 7115.
(6) Griffiths, R. B. *Phys. Rev. Lett.* **1969**, *23*, 17.
(7) Taniguchi, T.; Mizusaki, S.; Fukuoka, N.; Nagata, Y.; Noro, Y.; Samata, H. *J. Magn. Magn. Mater.* **2007**, *310*, 1067.
(8) Cao, G.; Chikara, S.; Lin, X. N.; Elhami, E.; Durairaj, V.; Schlottmann, P. *Phys. Rev. B* **2005**, *71*, 035104.
(9) Kolesnik, S.; Dabrowski, B.; Chmaissem, O. *Phys. Rev. B* **2008**, *78*, 214425.
(10) Yokoyama, M.; Satoh, C.; Saitou, A.; Kawanaka, H.; Bando, H.; Ohoyama, K.; Nishihara, Y. *J. Phys. Soc. Jpn.* **2005**, *74*, 1706.
(11) Woodward, P. M.; Goldberger, J.; Stoltzfus, M. W.; Eng, H. W.; Ricciardo, R. A.; Santhosh, P. N.; Karen, P.; Moodenbaugh, A. R. *J. Am. Ceram. Soc.* **2008**, *91*, 1976.
(12) Kennedy, B. J.; Zhou, Q. *Solid State Commun.* **2008**, *147*, 208.
(13) Kawanaka, H.; Yokoyama, M.; Noguchi, A.; Bando, H.; Nishihara, Y. *J. Phys.: Condens. Matter* **2009**, *21*, 296002.
(14) Taniguchi, T.; Mizusaki, S.; Okada, N.; Nagata, Y.; Lai, S. H.; Lan, M. D.; Hiraoka, N.; Itou, M.; Sakurai, Y.; Ozawa, T. C.; Noro, Y.; Samata, H. *Phys. Rev. B* **2008**, *77*, 014406.
(15) Shames, A. I.; Rozenberg, E.; Martin, C.; Maignan, A.; Raveau, B.; Andre, G.; Gorodetsky, G. *Phys. Rev. B* **2004**, *70*, 134433.
(16) Terai, K.; Yoshii, K.; Takeda, Y.; Fujimori, S.-I.; Saitoh, Y.; Ohwada, K.; Inami, T.; Okane, T.; Arita, M.; Shimada, K.; Namatame, H.; Taniguchi, M.; Kobayashi, K.; Kobayashi, M.; Fujimori, A. *J. Magn. Magn. Mater.* **2007**, *310*, 1070.
(17) Mizusaki, S.; Sato, J.; Taniguchi, T.; Nagata, Y.; Lai, S. H.; Lan, M. D.; Ozawa, T. C.; Noro, Y.; Samata, H. *J. Phys.; Condens. Matter* **2008**, *20*, 235242.

The behavior of these end members raises several interesting questions. Normally itinerant electron magnetism is favored with increasing tolerance factor, τ, because of the increased conduction bandwidth. Why then is $SrRu_{0.5}Mn_{0.5}O_3$ ($\tau = 0.987$) an insulating antiferromagnet and $CaRu_{0.5}Mn_{0.5}O_3$ ($\tau = 0.934$) an itinerant ferrimagnet? If both end members contain Mn^{3+}, why is a cooperative Jahn−Teller distortion seen for $SrRu_{0.5}Mn_{0.5}O_3$ but not $CaRu_{0.5}Mn_{0.5}O_3$? Is the crossover from antiferromagnetism to ferrimagnetism abrupt or are there intermediate states? To address these and other questions, we report here the electrical, magnetic, and structural properties of $Sr_{1-x}Ca_xRu_{0.5}Mn_{0.5}O_3$.

2. Experimental Section

2.1. Synthesis. All starting materials were dried for 24 h before use. Polycrystalline samples of 11 members in the series of $Sr_{1-x}Ca_xMn_{0.5}Ru_{0.5}O_3$ were prepared by the solid state reaction of the appropriate stoichiometric mixture of $SrCO_3$ (Aldrich 99.9+%), $CaCO_3$ (Aldrich, 99.95%), MnO_2 (Altheca 99.999%) and Ru (Altheca 99.9%). The powders, sufficient to make ca. 2 g of product, were well mixed using an agate mortar and heated in air first at 700 °C for 20 h, then at 1100 °C for 24 h and finally at 1150 °C for 6 days with intermediate regrindings. All calcination steps were carried out in alumina crucibles. Larger size samples, ca. 10 g, required for the neutron powder diffraction measurements were prepared following the same procedure.

2.2. Electrical and Magnetic Measurements. Linear four probe conductivity measurements were made between 10 and 300 K using a closed-cycle He-cryostat. Conducting silver paint was used to attach leads to regularly shaped bars which had densities ranging from 54 to 65% of their theoretical density; no corrections were made for porosity.

Magnetic data were collected with a LakeShore vibrating sample magnetometer (VSM). Sintered pellets ranging in mass from 15 to 40 mg were used for data collection. Samples were cooled to 80 K and a field of 500 G was applied. Zero-field-cooled (ZFC) measurements were gathered upon heating every 5 K from 80 to 350 K. Field-cooled (FC) data were collected upon cooling in a field of 500 G. Hysteresis measurements were made on samples at 80 K, cooled with zero-field, with a field oscillating between ±16 000 G while proceeding through zero. Additional field-cooled and zero-field-cooled measurements were made for two samples, $CaMn_{0.5}Ru_{0.5}O_3$ and $Sr_{0.5}Ca_{0.5}Mn_{0.5}Ru_{0.5}O_3$, using an MPMS XL Quantum Design SQUID magnetometer capable of reaching liquid helium temperatures. The zero field data were collected, after cooling, from 5 to 350 K in 5 K increments with a measuring field of 500 Oe. The field-cooled data were collected on cooling from 350 K in a field of 500 Oe.

AC magnetic susceptibility measurements (χ', χ'') were performed on a Quantum Design PPMS system in the temperature range 2−300 K ($CaMn_{0.5}Ru_{0.5}O_3$) and 2−350 K ($Ca_{0.5}Sr_{0.5}Mn_{0.5}Ru_{0.5}O_3$). AC field amplitude was 3 Oe and the frequency was varied between 10 and 10 000 Hz. No dc field was applied although there was a remnant field of about 0.1 Oe.

2.3. X-ray and Neutron Diffraction Studies. The sample purity was established through X-ray powder diffraction measurements using Cu−Kα radiation on a Shimadzu D-6000 Diffractometer. All samples were confirmed to contain only the desired perovskite phase. Synchrotron X-ray powder diffraction data were obtained with the Debye−Scherrer diffractometer on beamline 20B, the Australian National Beamline Facility (ANBF), at the Photon Factory, Tsukuba Japan.[18] Data were collected in 0.01° steps over the angular range $5° \le 2\theta \le 85°$ using two image plates as detectors. Each image plate is 20 × 40 cm and covers 40° in 2θ. The wavelength of the X-rays used was about 0.8 Å, accurately calibrated with Si 640c during each run. The samples were held in 0.3 mm diameter capillaries that rotated throughout the measurements. Temperatures up to 800 °C were achieved using a custom built furnace.

Neutron powder diffraction measurements were carried out with the constant wavelength ($\lambda = 1.538$ Å, $10° \le 2\theta \le 160°$) diffractometer Echidna at the OPAL reactor operated by the Australian Nuclear Science and Technology Organization [19]. The diffraction data were collected at room temperature and at 10 and 3 K for $CaMn_{0.5}Ru_{0.5}O_3$ and $Sr_{0.5}Ca_{0.5}Mn_{0.5}Ru_{0.5}O_3$, respectively. Magnetic and nuclear structures were refined using GSAS[20] or the combination of either SARAh[21] and GSAS or SARAh and FullProf,[22] giving virtually identical results.

2.4. X-ray Absorption Studies. X-ray absorption measurements were performed at the National Synchrotron Radiation Research Center (NSRRC) in Hsinchu, Taiwain.[23] Ru $L_{3,2}$-edge and Mn K-edge spectra were recorded in fluorescence mode on beamline BL-16A1 using a Lytle detector from powder samples dispersed on Kapton tape. Low-temperature measurements were performed using an ARS DE-202G Closed Cycle Cryostat. For these measurements, the powder samples were mixed with Apiezon Grease (Type N) and dispersed onto a copper plate in contact with the cryostat cold head. Energy steps as small as 0.2 eV were employed near the absorption edges with a counting time of 2 s per step. The spectra were normalized to the incident photon current. The energy scale of the Ru $L_{3,2}$- and Mn K-edge spectra was calibrated using the L_2-edge of a Mo foil and K-edge of a Mn foil respectively. Sr_2RuYO_6 and La_2MnRhO_6 were used as the Ru^{5+} and Mn^{3+} standards, and $SrRuO_3$ and $CaMnO_3$ as standards for Ru^{4+} and Mn^{4+}. Data analysis was carried out using a suite of programs within the software package EXAFSPAK [24]. First the BACKSUB program was used for background subtraction and normalization, followed by principal component analysis (PCA), target transformation (TARGET), and least-squares refinement (DATFIT).

3. Results

3.1. Electrical Conductivity. Variable-temperature electrical transport measurements were carried out on three representative samples of the $Sr_{1-x}Ca_xMn_{0.5}Ru_{0.5}O_3$ series, namely $SrMn_{0.5}Ru_{0.5}O_3$, $Sr_{0.5}Ca_{0.5}Mn_{0.5}Ru_{0.5}O_3$ and $CaMn_{0.5}Ru_{0.5}O_3$. The results are shown in Figure 2. The first thing to note is that none of the three samples show an abrupt change in conductivity in the vicinity of the magnetic ordering temperature. At room temperature the conductivities of the $SrMn_{0.5}Ru_{0.5}O_3$ and $CaMn_{0.5}Ru_{0.5}O_3$ samples

(18) Sabine, T. M.; Kennedy, B. J.; Garrett, R. F.; Foran, G. J.; Cookson, D. J. *J. Appl. Crystallogr.* **1995**, *28*, 513.
(19) Liss, K.-D.; Hunter, B.; Hagen, M.; Noakes, T.; Kennedy, S. *Physica B* **2006**, *385*−*386*, 1010.
(20) Toby, B. H. *J. Appl. Crystallogr.* **2001**, *34*, 210.
(21) Wills, A. S. *Physics B* **2000**, *276*, 680.
(22) Rodríguez-Carvajal, J. *Physica B* **1993**, *192*, 55.
(23) Dann, T. E.; Chung, S. C.; Huang, L. J.; Juang, J. M.; Chen, C. I.; Tsang, K. L. *J. Synchrotron Radiat.* **1998**, *5*, 664.
(24) George, G. N.; Pickering, I. J. *EAXFSPAK: A Suite of Computer Programs for Analysis of X-ray Absorption Spectra*; Stanford Synchrotron Radiation Laboratory: Menlo Park, CA, 2000.

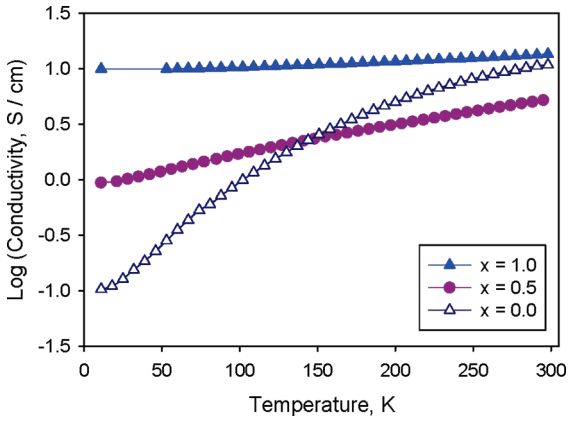

Figure 2. Electrical conductivity for $Sr_{1-x}Ca_xMn_{0.5}Ru_{0.5}O_3$ samples with $x = 0.0$, 0.5, and 1.0.

are nearly identical, $\sigma_{298K} \approx 10\ S\ cm^{-1}$, whereas the conductivity of the $Sr_{0.5}Ca_{0.5}Mn_{0.5}Ru_{0.5}O_3$ sample is slightly smaller ($\sigma_{298K} = 5.2\ S\ cm^{-1}$). The conductivities of these samples diverge from each other upon cooling. The conductivity of $CaMn_{0.5}Ru_{0.5}O_3$ shows little temperature dependence ($\sigma_{10K}/\sigma_{298K} = 0.73$). Despite the subtle decrease in conductivity for $CaMn_{0.5}Ru_{0.5}O_3$ on cooling, it is possible that the intrinsic conductivity is actually metallic in nature and that grain boundaries are responsible for the weak temperature dependence seen in Figure 2. The temperature dependence of related double perovskites, such as Sr_2FeMoO_6, have been shown to vary from metallic to slightly activated depending upon the sintering conditions and grain boundaries.[25]

In contrast, the conductivity of $SrMn_{0.5}Ru_{0.5}O_3$ drops by 2 orders of magnitude over the same temperature interval. Despite the relatively low density of the ceramic pellet, the temperature dependent conductivity of this sample is in qualitative agreement with single crystal measurements on $SrMn_{0.59}Ru_{0.41}O_3$, where the conductivity decreases from ~50 S cm^{-1} at room temperature to ~0.01 S cm^{-1} at ~4 K.[8] Both the single-crystal study and an earlier measurement on sintered pellets of $SrMn_{0.5}Ru_{0.5}O_3$ [11] successfully modeled the temperature dependence with a variable range hopping model. The conductivity of $Sr_{0.5}Ca_{0.5}Mn_{0.5}Ru_{0.5}O_3$ is intermediate, dropping by a factor of ~5 over the same temperature interval.

3.2. Magnetic Measurements. The magnetic susceptibility of $SrMn_{0.5}Ru_{0.5}O_3$ peaks on cooling, indicating antiferromagnetic ordering with a Néel temperature of ~215 K (Figure 3a). $Sr_{0.9}Ca_{0.1}Mn_{0.5}Ru_{0.5}O_3$ shows similar behavior with a peak that is broadened and shifted to slightly lower temperature, $T_N \approx 190$ K. These observations are consistent with previous studies that have shown that $SrMn_{0.5}Ru_{0.5}O_3$ adopts the antiferromagnetic C-type structure below ~200 K.[9−11]

As the calcium content increases the antiferromagnetic behavior gives way to ferromagnetic/ferrimagnetic behavior for $x \geq 0.2$ (Figure 3b). As shown in Figure 4 the T_C is close to room temperature until $x = 0.7$. For higher levels

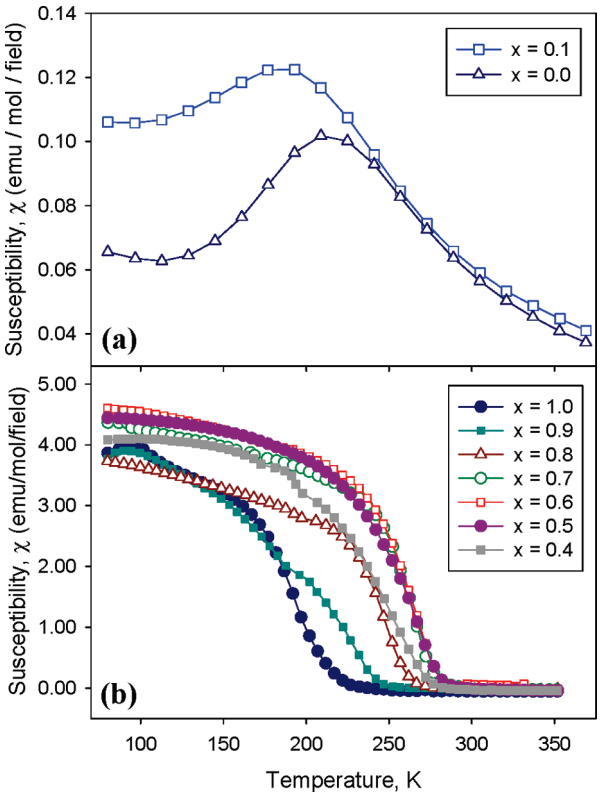

Figure 3. Magnetization versus temperature curves for $Sr_{1-x}Ca_xMn_{0.5}Ru_{0.5}O_3$, (a) for $x = 0$ and 0.1 and (b) $x \geq 0.4$. For clarity, the weaker ferromagnetic curves for $x = 0.2$, 0.3 are omitted.

of calcium substitution T_C drops off, reaching a value of 230 K in $CaMn_{0.5}Ru_{0.5}O_3$. The M vs H plot for $CaMn_{0.5}Ru_{0.5}O_3$ (Figure 5) shows hysteretic behavior confirming the ferromagnetic/ferrimagnetic nature of the sample. Similar plots were seen for all of the samples with $x > 0.2$. Values of saturation magnetization, M_{sat}, ranged from 0.55−0.82 μ_B/formula unit for all samples with $x > 0.3$. These values represent a robust ferromagnetism/ferrimagnetism, which cannot be explained by a weakly canted antiferromagnetic state, or the presence of an undetected ferromagnetic impurity, such as $SrRuO_3$ ($T_C = 165$ K) [25,26]. On the other hand, the values of M_{sat} are smaller than might be expected for full ferromagnetic alignment of manganese and ruthenium spins. Simple-minded arguments based on localized electrons and a 50:50 mixture of Mn^{3+} (d^4) and Ru^{5+} (d^3) predict $1/2(4 + 3) \approx 3.5\ \mu_B$/formula unit. Similar arguments based on a 50:50 mixture of Mn^{4+} (d^3) and Ru^{4+} (low-spin d^4) would suggest a somewhat smaller moment of $1/2(3 + 2) \approx 2.5\ \mu_B$/formula unit. A ferrimagnetic alignment of the Mn and Ru moments in either valence couple would result in M_{sat} of $1/2(4-3) \approx 1/2(3-2) \approx 0.5\ \mu_B$/formula unit. Thus saturation magnetization measurements lend support for a ferrimagnetic ground state, as suggested by magnetic Compton scattering and XMCD. As discussed later, the fact that the saturation magnetization is larger than 0.5 μ_B/formula unit is thought to result from a reduced moment on ruthenium. All samples had

(25) Huang, Y. H.; Karppinen, M.; Yamauchi, H.; Goodenough, J. B. *Phys. Rev. B* **2006**, *73*, 104408.

(26) Longo, J. M.; Raccah, P. M.; Goodenough, J. B. *J. Appl. Phys.* **1968**, *39*, 1327.

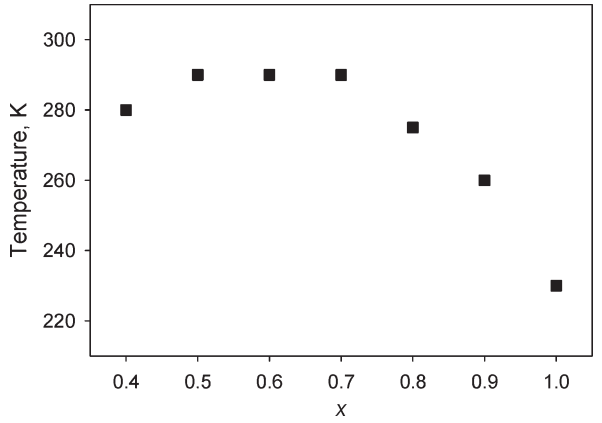

Figure 4. A plot of T_C vs x for $x \geq 0.4$.

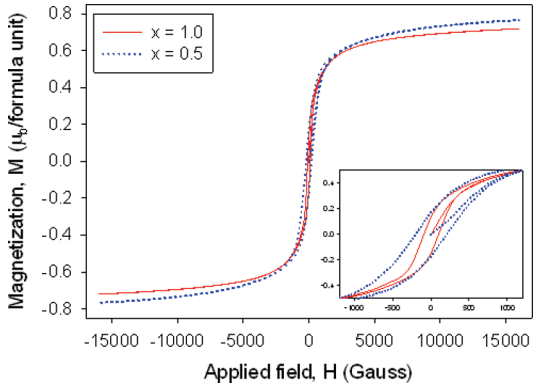

Figure 5. Magnetization (M) vs applied field (H) curves for $CaMn_{0.5}Ru_{0.5}O_3$ (line) and $Sr_{0.5}Ca_{0.5}Mn_{0.5}Ru_{0.5}O_3$ (dots) collected at 80 K.

small coercivities, between 650 and 200 G, decreasing as the amount of calcium increases.

Field-cooled and zero-field-cooled data were collected down to liquid helium temperatures on a SQUID magnetometer for $Sr_{0.5}Ca_{0.5}Mn_{0.5}Ru_{0.5}O_3$ and $CaMn_{0.5}Ru_{0.5}O_3$. The susceptibility vs temperature plots are shown in Figure 6. Both samples display paramagnetic to ferromagnetic transitions on cooling. The $Sr_{0.5}Ca_{0.5}Mn_{0.5}Ru_{0.5}O_3$ sample shows a smooth divergence between FC and ZFC data typical of other reports on $AMn_{1-x}Ru_xO_3$ perovskites [11,27]. Presumably it is related to the lack of long-range Mn/Ru order, which can lead to the formation of magnetic clusters. In the related $CaMn_{1-x}Ir_xO_3$ system similar behavior has been attributed to the formation of ferromagnetic clusters [28]. The χ vs T plot for $CaMn_{0.5}Ru_{0.5}O_3$ (Figure 6b) is intriguing. An unexpected peak is observed at ~95 K, signaling the onset of a more dramatic FC vs ZFC divergence.

Magnetic AC susceptibility measurements were collected for both samples and $\chi'(T)$ plots are shown in Figure 7. For both samples a sharp rise in $\chi'(T)$ at T_C = 290 K for $Sr_{0.5}Ca_{0.5}Mn_{0.5}Ru_{0.5}O_3$ and T_C = 230 K for $CaMn_{0.5}Ru_{0.5}O_3$ is consistent with the DC magnetic

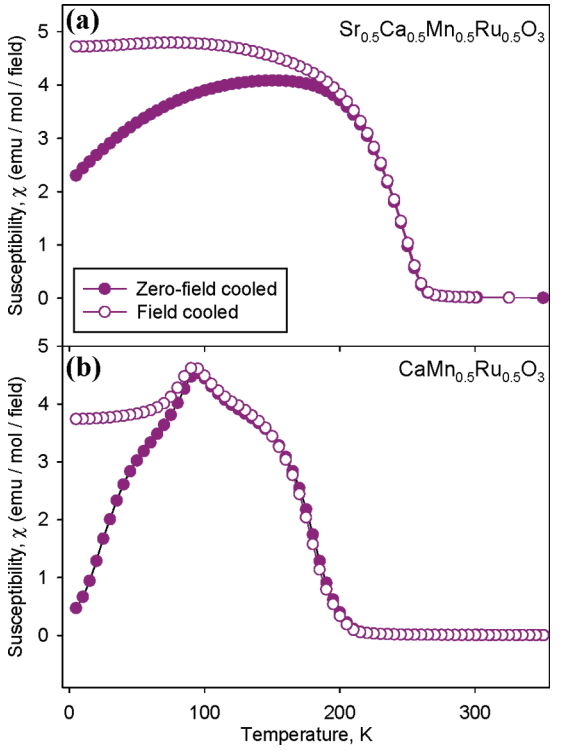

Figure 6. Magnetic susceptibility vs temperature for (a) $Sr_{0.5}Ca_{0.5}Mn_{0.5}Ru_{0.5}O_3$ and (b) $CaMn_{0.5}Ru_{0.5}O_3$.

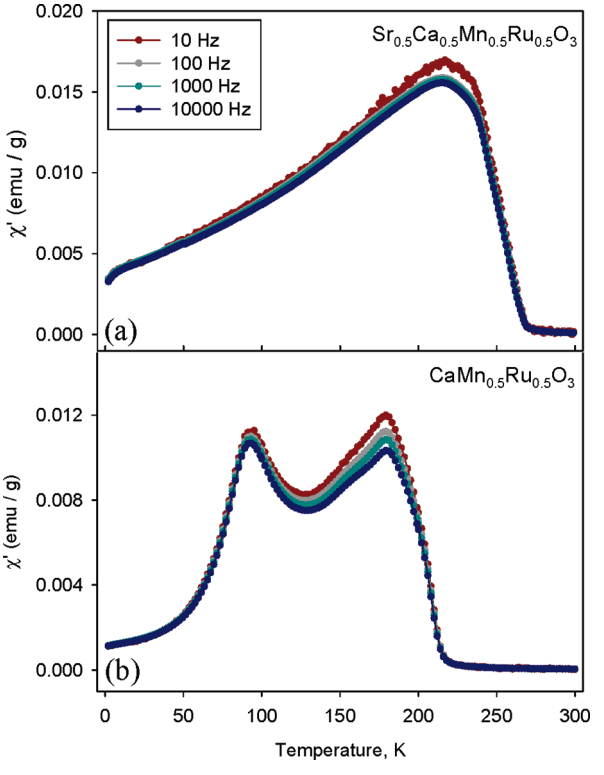

Figure 7. AC magnetic susceptibility vs temperature for (a) $Sr_{0.5}Ca_{0.5}Mn_{0.5}Ru_{0.5}O_3$ and (b) $CaMn_{0.5}Ru_{0.5}O_3$.

susceptibility measurements. In both cases the AC χ' (T) curves do not show a single sharp peak, as would be expected for a single magnetic transition in a magnetically homogeneous sample. In particular, $CaMn_{0.5}Ru_{0.5}O_3$ clearly exhibits a distinct second magnetic transition

(27) Dass, R. I.; Yan, J.-Q.; Goodenough, J. B. *Phys. Rev. B* **2004**, *69*, 094416.
(28) Mizusaki, S.; Sato, J.; Taniguchi, T.; Nagata, Y.; Lai, S. H.; Lan, M. D.; Ozawa, T. C.; Noro, Y.; Samata, H. *J. Phys.: Condens. Matter* **2008**, *20*, 235242.

Table 1. Space Group Symmetry and Unit-Cell Dimensions of $Sr_{1-x}Ca_xMn_{0.5}Ru_{0.5}O_3$ for $0 \leq x \leq 1$

	x					
	0	0.1	0.2	0.3	0.3	0.4
space group	*I*4/*mcm*	*I*4/*mcm*	*I*4/*mcm*	*I*4/*mcm*	*Pnma*	*Pnma*
a (Å)	5.4587(3)	5.4450(1)	5.4362(2)	5.4326(1)	5.4661(2)	5.4580(1)
b (Å)					7.7264(2)	7.7144(2)
c (Å)	7.9193(4)	7.9200(2)	7.8946(3)	7.8789(2)	5.4756(2)	5.4678(2)
R_p	9.22	7.24	6.31	4.77	4.77	4.14
R_{wp}	13.59	10.10	9.94	6.11	6.11	5.01
	x					
	0.5	0.6	0.7	0.8	0.9	1.0
space group	*Pnma*	*Pnma*	*Pnma*	*Pnma*	*Pnma*	*Pnma*
a (Å)	5.4467(3)	5.4323(5)	5.4162(2)	5.4068(3)	5.4322(3)	5.4305(1)
b (Å)	7.6984(3)	7.6767(3)	7.6619(2)	7.6271(4)	7.6058(4)	7.5870(2)
c (Å)	5.4494(3)	5.4324(5)	5.4083(2)	5.3896(2)	5.3650(3)	5.3403(1)
R_p	4.02	6.42	6.53	8.22	5.13	3.29
R_{wp}	5.66	10.22	9.91	12.18	7.84	4.56

below 100 K, which is likely indicative of magnetic phase separation.

3.3. X-ray Powder Diffraction. All samples adopt distorted variants of the simple ABO_3 perovskite structure. The space group and unit-cell dimensions of each sample were established by considering both the splitting of the parent perovskite Bragg reflections and the nature of the superlattice reflections associated with cooperative tilting of the octahedra. Once the space group was established the structure of each member was refined using the Rietveld method. The space group symmetry and unit-cell dimensions are included in Table 1. At the outset we note that the X-ray diffraction patterns did not provide any evidence for long-range ordering of the Ru and Mn cations on the B-site. Neither was evidence for ordering of Ru and Mn found in the neutron diffraction studies, described in the next section, nor was it possible to find compelling evidence for Mn/Ru order in selected area electron diffraction patterns (not reported). Thus we can say with certainty that there is no long-range three-dimensional ordering of Mn and Ru in any of the samples investigated.

The structures of the Sr-rich samples, $x < 0.3$, are tetragonal and possess *I*4/*mcm* space group symmetry. This space group allows for both out-of-phase rotations of the octahedra about the *c*-axis ($a^0a^0c^-$ tilting), as well as a cooperative Jahn−Teller distortion (CJTD) of the octahedra (Figure 8). Although the (Mn/Ru)−O bonds running parallel to the *c*-axis remain linear, those lying in the *ab*-plane are bent as a result of the octahedral tilting. Evidence for a cooperative Jahn−Teller distortion can be found in the bond distances that define the $(Mn/Ru)O_6$ octahedra. As previously reported the Mn/Ru−O distances as obtained from synchrotron XRD studies of $SrMn_{0.5}Ru_{0.5}O_3$ are 1.942(1) Å (× 4) for the bonds in the *ab*-plane and 1.980(1) Å (× 2) for the bonds that lie parallel to the *c*-axis [12]. Octahedral tilting reduces the (Mn/Ru)−O−(Mn/Ru) bond angle in the *ab*-plane from 180 to 166.4(4)°. These values are in good agreement with

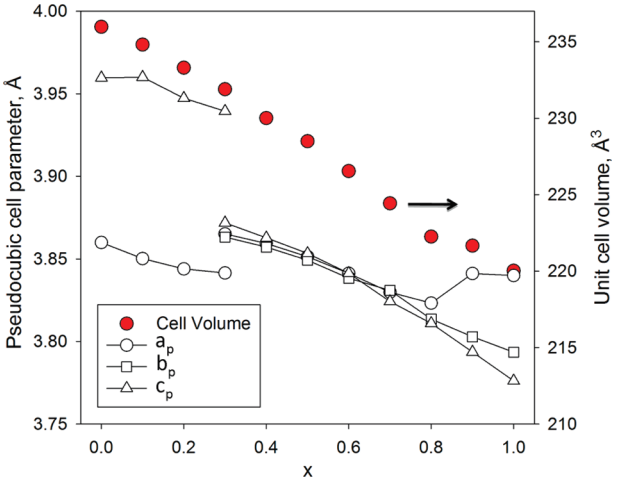

Figure 8. Reduced cell parameters (*Pnma*, $a_p = a/\sqrt{2}$, $b_p = b/2$, $c_p = c/\sqrt{2}$; *I*4/*mcm*, $a_p = b_p = a/\sqrt{2}$, $c_p = c/2$) for $Sr_{1-x}Ca_xMn_{0.5}Ru_{0.5}O_3$. The uncertainties associated with these parameters are smaller than the symbols used to plot the data points. The larger filled circles are the unit-cell volume as a function of *x*. Note the coexistence of the tetragonal and orthorhombic phases at $x = 0.3$.

previous neutron powder diffraction studies [9,11,29]. The synchrotron X-ray diffraction patterns of the tetragonal perovskites were also characterized by anisotropic peak broadening that was modeled in the Rietveld refinements by broadening the 00*l* type reflections. We believe that this broadening is a consequence of the disorder that exists between the Jahn−Teller distorted MnO_6 and more symmetric RuO_6 octahedra.

At higher Ca contents, the peak splitting seen for the tetragonal distortion is dramatically reduced, and superlattice reflections appear that are indicative of the existence of both in- and out-of-phase tilting of the octahedra. The space group symmetry is *Pnma*, as previously reported for $CaRu_{0.5}Mn_{0.5}O_3$[29] as well for $CaRuO_3$[30] and $CaMnO_3$.[31] In perovskites, this symmetry generally

(29) Lufaso, M. W.; Woodward, P. M.; Goldberger, J. *J. Solid State Chem.* **2004**, *177*, 1651.
(30) Ranjan, R.; Senyshyn, A.; Vashook, V.; Niewa, R.; Boysen, H.; Frey, F. *Appl. Phys. Lett.* **2007**, *90*, 251913.
(31) Bozin, E. S.; Sartbaeva, A.; Zheng, H.; Wells, S. A.; Mitchell, J. F.; Proffen, Th.; Thorpe, M. F.; Billinge, S. J. L. *J. Phys. Chem. Solids* **2008**, *69*, 2146.
(32) Woodward, P. M. *Acta Crystallogr., Sect. B* **1997**, *53*, 32.

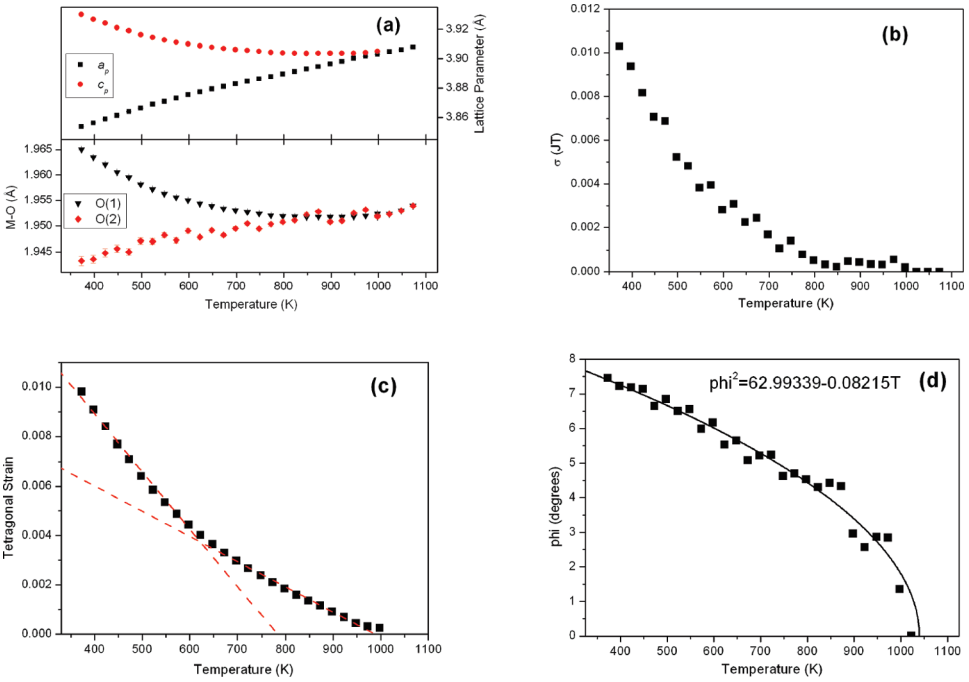

Figure 9. Results from a variable-temperature X-ray diffraction study of $Sr_{0.8}Ca_{0.2}Mn_{0.5}Ru_{0.5}O_3$ showing: (a) the anisotropy of the Mn/Ru−O bond distances, (b) the Jahn−Teller distortion parameter defined in Radaelli et al.,[35] (c) the tetragonal strain, and (d) the octahedral tilt angle phi, φ.

results from $a^-b^+a^-$ tilting.[32−34] The structures of the oxides with $x > 0.3$ were refined using this space group. Two features emerged from the structural refinements; first, the anisotropic broadening observed in the tetragonal oxides was no longer present, and second, the bond length anisotropy was effectively absent. These two features combined indicate either a loss of, or at least a change in the type of, orbital order.

Fits to the X-ray diffraction pattern of the $x = 0.3$ sample were unsatisfactory when using single-phase models in either *Pnma* or *I*4/*mcm*. Ultimately, an acceptable fit was obtained using a model that contained a mixture of these two phases, with 73.5(2)% of the sample adopting the orthorhombic structure. The coexistence of these two phases is consistent with a first-order transition between the orthorhombic and tetragonal structures. Group theory shows that a *Pnma*−*I*4/*mcm* transition must be first order in ABO_3 perovskites.[34]

Figure 8 illustrates the reduced lattice parameters as a function of x. In general terms four distinct regions can be identified:

(a) $0 \le x \le 0.2$, a tetragonal region where the space group symmetry is *I*4/*mcm* and the unit cell is clearly distorted by a CJTD;

(b) $0.2 < x < 0.4$, a two-phase region;

(c) $0.4 \le x \le 0.7$, a pseudocubic region where the space group symmetry is *Pnma* but the unit cell is highly pseudocubic;

(d) $0.7 < x \le 1.0$, an orthorhombic region where the space group symmetry is *Pnma* and the orthorhombic distortion of the unit cell can clearly be seen.

Variable-temperature studies have been carried out on four representative samples. As described in a recent communication the CJTD in $SrRu_{0.5}Mn_{0.5}O_3$ disappears above ~523 K, signifying a loss of orbital order, and the $a^0a^0c^-$ tilting disappears above ~673 K, where the structure transforms from tetragonal to cubic [12]. The temperature dependent behavior of the isostructural $Sr_{0.8}Ca_{0.2}Mn_{0.5}Ru_{0.5}O_3$ sample shows similar characteristics. By following the anisotropy in the Mn/Ru−O bond distances (Figure 9a) we see that the cooperative Jahn−Teller distortion disappears above 800 K, whereas the tetragonal symmetry persists to ~1000 K, as demonstrated by both the loss of any discernible intensity associated with the strongest of the R-point reflections (i.e., the 121 near $2\theta = 19.7°$ for $\lambda = 0.798$ Å) and a progressive decrease in the diagnostic tetragonal splitting (Figure 9(a)). This change occurs at the same temperature that noticeable distortion of the Ru/MnO_6 octahedra vanishes (Figure 9b). The postulate that the transition to cubic occurs in two steps is confirmed from the spontaneous strains in which two linear regions are observed (Figure 9c). The first corresponds to the removal of the CJTD and the second to the removal of the octahedral tilting. The removal of the tilts appears to be second order and within the precision of the data the tilt angle, φ, was unaffected by the loss of the CJTD (Figure 9d). The persistence of the R-point reflection up to ~1000 K unequivocally demonstrates out-of-phase rotations of the octahedra at that temperature despite the unit cell being metrically cubic.

As noted above, the diffraction pattern for the sample with $x = 0.3$ was best fitted using a two-phase model in

(33) Woodward, P. M. *Acta Crystallogr., Sect. B* **1997**, *53*, 44.
(34) Howard, C. J.; Stokes, H. T. *Acta Crystallogr., Sect. B* **1998**, *54*, 782.
(35) Radaelli, P. G.; Iannone, G.; Marezio, M.; Hwang, H. Y.; Cheong, S.-W.; Jorgensen, J. D.; Argyriou, D. N. *Phys. Rev. B* **1997**, *56*, 8265.

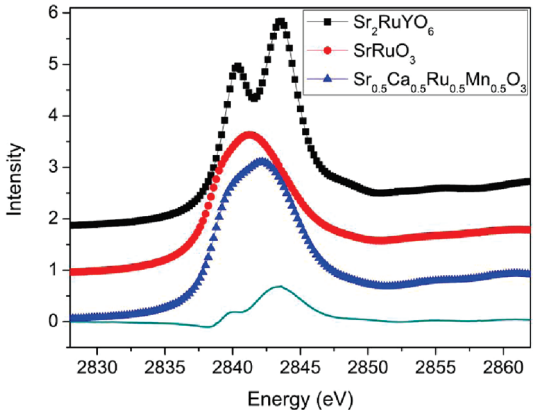

Figure 10. Normalized Ru L_3-edge absorption spectra of $Ca_{0.5}Sr_{0.5}Mn_{0.5}Ru_{0.5}O_6$ and the Ru^{4+} and Ru^{5+} standard materials. The spectra are offset in the *y*-axis for clarity. The dashed line is the difference spectrum obtained by subtracting the spectrum of $SrRuO_3$ from that of $Ca_{0.5}Sr_{0.5}Ru_{0.5}Mn_{0.5}O_3$. The shift to higher energy of the Ru L_3-edge in $Ca_{0.5}Sr_{0.5}Ru_{0.5}Mn_{0.5}O_3$ vs $SrRuO_3$ is evident from the derivative like shape of the difference spectrum.

which the tetragonal and orthorhombic phases coexist. Heating the sample to 773 K did not result in the formation of a single phase sample. The coexistence of the tetragonal and orthorhombic phases over a wide temperature interval can be partially ascribed to the large strains in the tetragonal phase, and we postulate that the observed phase segregation reflects the different electronic structures of the two oxides, with the tetragonal, but not the orthorhombic, phase exhibiting CJTD. Electronic phase segregation can occur in perovskite manganites as a consequence of the strains resulting from the differences in the lattice parameters of the distinct electronic phases.[36] The temperature dependence of the lattice parameters of the orthorhombic phase were unremarkable, simply increasing as the temperature was increased. This is in contrast to the marked temperature dependence of the lattice parameters of the tetragonal phase which are very similar to that seen for the $x = 0.2$ sample described above.

The final sample examined using high- temperature synchrotron XRD was $Sr_{0.5}Ca_{0.5}Ru_{0.5}Mn_{0.5}O_3$. As discussed above this sample is highly pseudocubic and the diffraction pattern shows little splitting of the strongest Bragg reflection at any temperature. However the pattern does exhibit a number of R- and M-point reflections indicative of the presence of both in-phase and out-of-phase tilts of the octahedra. The orthorhombic symmetry as well as the pseudocubic cell parameters are retained up to the highest temperature measured, 1073 K.

3.4. X-ray Absorption Studies. The Ru L-edge XANES spectra are known to be sensitive to the formal oxidation state of the Ru cations. The spectra for the L_2 and L_3 edges were very similar and therefore we present results only for the lower energy L_3 lines. As reported by previous researchers,[37,38] we observed that the Ru L-edge spectrum for the Ru^{5+} standard studied (Sr_2RuYO_6) is characterized by a well-resolved doublet arising from the transition from the Ru 2p to 4d orbitals, where separate transitions to the t_{2g} and e_g orbitals are resolved. By comparison, the Ru L-edge spectrum for the Ru^{4+} standard ($SrRuO_3$) comprises a poorly resolved doublet, reflecting the smaller crystal field splitting associated with Ru^{4+}. At the same time, the Ru L-edge appears at higher energy in the Ru^{5+} oxides than it does in the Ru^{4+} oxides. Superficially, the shape of the Ru L_3-edge XANES spectra of various $Sr_{1-x}Ca_xRu_{0.5}Mn_{0.5}O_3$ perovskites resemble that of the Ru^{4+} standard; however, careful examination suggests a combination of Ru^{4+} and Ru^{5+} in all samples (see example of $Sr_{0.5}Ca_{0.5}Ru_{0.5}Mn_{0.5}O_3$ in Figure 10). Furthermore, the edge position of all samples is intermediate between that of the Ru^{5+} and Ru^{4+} standards indicating that the Ru in the $Sr_{1-x}Ca_xRu_{0.5}Mn_{0.5}O_3$ oxides, formally, have a noninteger valence. This observation is consistent with the report by Sahu and co-workers,[39] who concluded that the Ru in $SrRu_{0.5}Mn_{0.5}O_3$ has an effective average oxidation state of ~4.5, although unlike Bos and co-workers,[40] they did not quantify this.

Of greater interest in the current work is the possibility that the extent of Ru/Mn charge transfer is sensitive to the precise Ca:Sr ratio. Although the spectra are all very similar, we observe a small but systematic broadening of the L_3-edge spectra with increasing Ca content. At the same time, there is a small enhancement in the resolution of the Ru L_3-edge spectra that is indicative of a greater Ru^{5+} character in $SrRu_{0.5}Mn_{0.5}O_3$. This is best illustrated when the spectra of the two end-members are compared as shown in Figure 11a.

These conclusions are confirmed by quantitative analysis of the Ru L_3-edge XANES spectra using the software package EXAFSPAK [24]. First principal component analysis (PCA) of the $Sr_{1-x}Ca_xRu_{0.5}Mn_{0.5}O_3$ series was performed over the energy range of 2800−2900 eV (corresponding to the Ru L_3-edge), using the PCA program belonging to the EXAFSPAK suite. This analysis suggested that there were only two significant components in the spectra of $Sr_{1-x}Ca_xRu_{0.5}Mn_{0.5}O_3$ ($x = 0-1$). Target transformation analysis (TARGET) further demonstrated that the Ru^{4+} and Ru^{5+} standards ($CaRuO_3$ and Sr_2RuYO_6) were suitable choices as those two components. The Ru L_3-edge XANES spectra of the $Sr_{1-x}Ca_xRu_{0.5}Mn_{0.5}O_3$ samples were then fitted to a linear combination of the two standard materials over the energy range of 2800−2900 eV, using a least-squares refinement program (DATFIT). The derived Ru oxidation states are listed in Table 2, showing a general trend of decreased Ru valence with increasing Ca content.

To confirm that the shift in the Ru L-edge spectra is a consequence of an increase in the Ru to Mn charge transfer,

(36) Sage, M. H.; Blake, G. R.; Nieuwenhuys, G. J.; Palstra, T. T. M. *Phys. Rev. Lett.* **2006**, *96*, 036401.
(37) Hu, Z.; von Lips, H.; Golden, M. S.; Fink, J.; Kaindl, G.; de Groot, F. M. F.; Ebbinghaus, S.; Reller, A. *Phys. Rev. B.* **2000**, *61*, 5262.
(38) Liu, R. S.; Jang, L. Y.; Hung, H. H.; Tallon, J. L. *Phys. Rev. B.* **2001**, *63*, 212507.
(39) Sahu, R. K.; Hu, Z.; Rao, M. L.; Manoharan, S. S.; Schmidt, T.; Richter, B.; Knupfer, M.; Golden, M.; Fink, J.; Schneider, C. M. *Phys. Rev. B* **2002**, *66*, 144415.
(40) Bos, J.-W. G.; Attfield, J. P.; Chan, T.-S.; Liu, R.-S.; Jang, L.-Y. *Phys. Rev. B* **2005**, *72*, 014101.

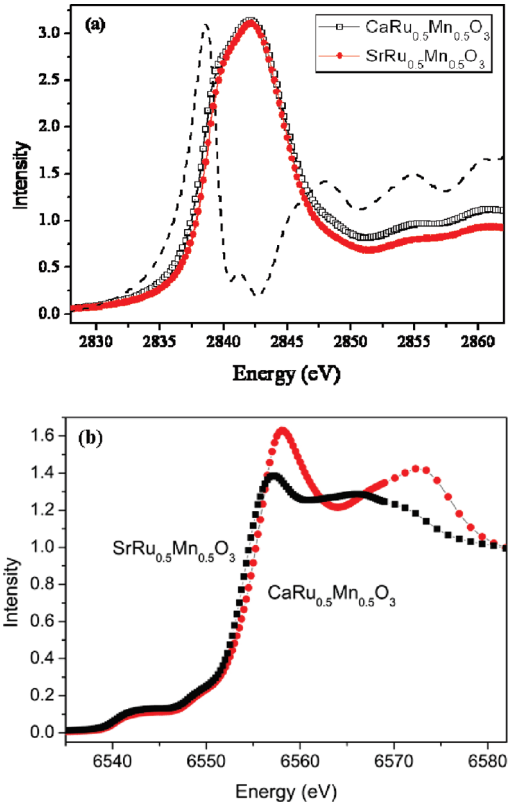

Figure 11. Normalized (a) Ru L_3-edge, and (b) Mn K-edge absorption spectra for $CaMn_{0.5}Ru_{0.5}O_3$ and $SrMn_{0.5}Ru_{0.5}O_3$. Notice that $CaMn_{0.5}Ru_{0.5}O_3$ shows a shift to lower energy (see difference spectrum, rescaled for clarity) in the Ru L_3-edge spectrum and a shift to higher energy in the Mn K-edge spectrum. These changes indicate a shift toward Ru^{4+}/Mn^{4+} as the Ca content increases.

Table 2. Ru Oxidation State in $Sr_{1-x}Ca_xRu_{0.5}Mn_{0.5}O_3$ as Derived from the Ru L_3-Edge XANES Spectra

	x										
	0	0.1	0.2	0.3	0.4	0.5	0.6	0.7	0.8	0.9	1.0
Ru valence	4.45	4.43	4.42	4.42	4.30	4.32	4.33	4.22	4.24	4.16	4.16

we recorded Mn K-edge spectra for the two end-members, $CaRu_{0.5}Mn_{0.5}O_3$ and $SrRu_{0.5}Mn_{0.5}O_3$, as illustrated in Figure 11b. The edge position of $CaRu_{0.5}Mn_{0.5}O_3$ is shifted to higher energy indicative of an increase in the Mn valence state. This shift is opposite to that seen for the Ru L-edge spectra demonstrating electron transfer between Ru and Mn. The Mn K-edge absorption spectra were also fitted, giving rise to a Mn valence of 3.44 for $SrMn_{0.5}Ru_{0.5}O_3$ and 3.65 for $CaMn_{0.5}Ru_{0.5}O_3$. We note that the absence of suitable standards, having Mn environments similar to the system being studied, limits the accuracy of these values.

3.2. Neutron Powder Diffraction Studies. Neutron powder diffraction data were collected for two compounds, $CaMn_{0.5}Ru_{0.5}O_3$ and $Sr_{0.5}Ca_{0.5}Mn_{0.5}Ru_{0.5}O_3$, to more accurately locate the position of the oxygen atoms and to probe for any sign of Sr/Ca and/or Mn/Ru order. The coherent scattering lengths of the cations, 4.70 fm (Ca), 7.02 fm (Sr), −3.73 fm (Mn), and 7.03 fm (Ru), provide a large contrast that is sensitive to chemical ordering, particularly for the Mn/Ru pair. Data were collected at both room temperature and low temperature. The nuclear structures were refined using the Rietveld method, first on the room temperature data (shown in Figure 12) and then on the low temperature data, where the magnetic structure also comes into play.

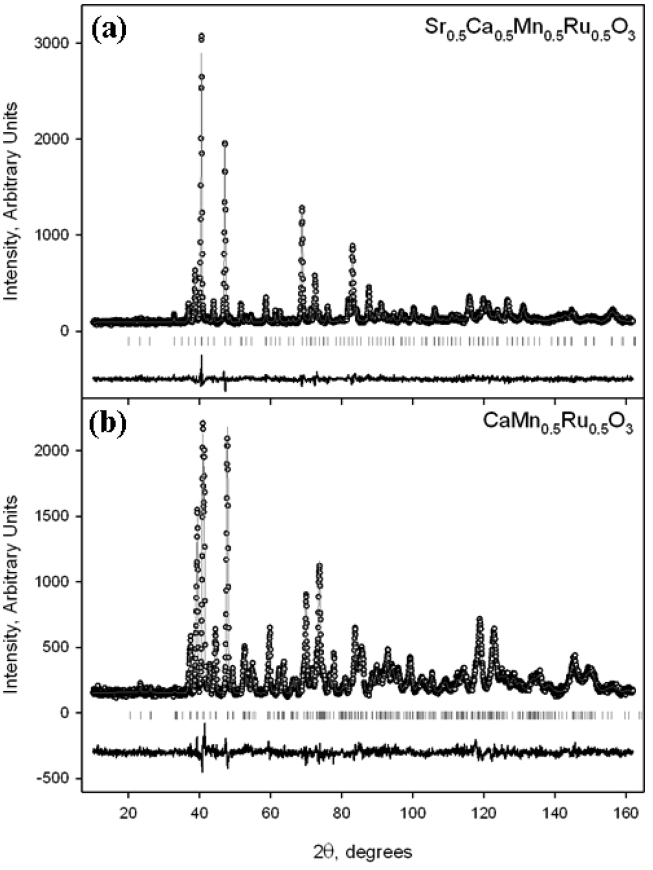

Figure 12. Rietveld refinements for (a) $Sr_{0.5}Ca_{0.5}Mn_{0.5}Ru_{0.5}O_3$ and (b) $CaMn_{0.5}Ru_{0.5}O_3$ using NPD data collected at room temperature. The observed data points are plotted with open circles and the calculated pattern with a gray line. The difference between the calculated and observed is shown at the bottom and the vertical marks indicate positions for allowed reflections.

Both materials were refined with *Pnma* space group symmetry. The lattice parameters and atomic positions are shown in Table 3. The structure refinements gave no indication that these materials are nonstoichiometric or deviate from the nominal oxygen content and there is no evidence for long-range chemical order of Mn and Ru. From the atomic positions there is no doubt that the structure of $Sr_{0.5}Ca_{0.5}Mn_{0.5}Ru_{0.5}O_3$ has orthorhombic symmetry. Nonetheless, the pseudocubic cell metric seen in the X-ray data is also apparent in the neutron data.

As mentioned above, introduction of a magnetic phase was necessary to model the low temperature data. The magnetic phases were generated with the program SARAh. The magnetic structures of these two samples could be modeled in two different ways. One approach is to assume that the magnetic structure is homogeneous throughout the sample and model the magnetic structure using one of the irreducible representations (irreps) provided by SARAh. This approach led to satisfactory fits using any of the irreps that possess a ferromagnetic component. In all

Table 3. Rietveld Refinement Results for $Sr_{1-x}Ca_xMn_{0.5}Ru_{0.5}O_3$ (x = 0.5, 1) as Obtained from Analysis of Neutron Powder Diffraction Data

	$Sr_{0.5}Ca_{0.5}Mn_{0.5}Ru_{0.5}O_3$		$CaMn_{0.5}Ru_{0.5}O_3$	
T (K)	298	3	298	10
space group	*Pnma*	*Pnma*	*Pnma*	*Pnma*
a (Å)	5.4477(6)	5.4494(4)	5.4198(3)	5.4124(2)
b (Å)	7.6996(7)	7.6981(4)	7.5854(4)	7.5627(3)
c (Å)	5.4481(8)	5.4473(4)	5.3395(3)	5.3192(2)
R_p	7.57	6.14	6.23	5.26
R_{wp}	9.78	7.97	7.86	6.67
χ^2	1.459	5.596	1.599	2.863
$R(F^2)$	7.96	9.89	6.51	7.04
Ca/Sr x	0.5161(8)	0.5219(6)	0.5433(5)	0.5463(5)
y	1/4	1/4	1/4	1/4
z	0.511(1)	0.507(1)	0.5086(8)	0.5080(7)
$U_{iso} \times 100$	0.99(7)	0.50(4)	0.89(5)	1.00(5)
Ru/Mn	(1/2, 0, 0)	(1/2, 0, 0)	(1/2, 0, 0)	(1/2, 0, 0)
$U_{iso} \times 100$	2.6(2)	2.7(1)	0.5(1)	0.3(1)
O(1) x	−0.006(1)	−0.0096(9)	−0.0178(4)	−0.0207(4)
y	1/4	1/4	1/4	1/4
z	0.453(1)	0.439(1)	0.4321(5)	0.4187(4)
$U_{iso} \times 100$	1.67(7)	1.70(9)		
U_{eqv}[a]			1.25	1.98
O(2) x	0.2795(7)	0.2796(6)	0.2941(3)	0.2951(3)
y	0.0335(6)	0.0305(5)	0.0406(2)	0.0410(2)
z	0.7151(7)	0.7154(5)	0.7043(3)	0.7041(3)
$U_{iso} \times 100$	1.80(6)	1.34(5)		
U_{eqv}[a]			3.06	2.77
Mn magnetic moment (μ_B)		+3.45		+3.33
Ru magnetic moment (μ_B)		−1.04(9)		−1.14(7)

[a] Refined anisotropic U values are as follows: O(1), U_{11} = 1.5(1), U_{22} = 0.1(1), U_{33} = 0.3(1), U_{12} = 0, U_{13} = 0.08(7), U_{23} = 0; O(2), U_{11} = 1.72(7), U_{22} = 1.01(8), U_{33} = 0.56(5), U_{12} = 0.06(7), U_{13} = −0.11(8), U_{23} = −0.47(8).

cases the ferromagnetic contribution was dominant, but it should be noted that a slightly better fit was always obtained by introducing an antiferromagnetic contribution. Hence the best solutions correspond to a structure where the moments are canted away from a simple ferromagnetic alignment.

An alternative approach is to assume the magnetic ordering is inhomogeneous and model the data using two magnetic phases, one ferromagnetic and the other antiferromagnetic. The two approaches to modeling the magnetic Bragg reflections give essentially identical fits, and therefore cannot be distinguished from each other. However, the ac susceptibility data as well as previous reports in the literature [13,15] on $CaMn_{1-x}Ru_xO_3$ point toward the two-phase explanation. Hence, this is the model reported here.

Figure 13 shows the low-angle regions of the neutron diffraction patterns for both $CaMn_{0.5}Ru_{0.5}O_3$ and $Sr_{0.5}Ca_{0.5}Mn_{0.5}Ru_{0.5}O_3$. Calculated patterns are shown for refinements where we attempted to fit the magnetic peaks using a simple (noncanted) single phase magnetic structure. Notice that although a ferromagnetic solution accounts for much of the increased peak intensity seen at low temperature, there are magnetic scattering contributions that cannot be accounted using a simple ferromagnetic model. In the case of $CaMn_{0.5}Ru_{0.5}O_3$, the presence of the orthorhombic (110) peak indicates a contribution from an antiferromagnetic G-type phase, whereas in the case of $Sr_{0.5}Ca_{0.5}Mn_{0.5}Ru_{0.5}O_3$ the (100) peak indicates a contribution from an antiferromagnetic C-type phase.

Because of correlations, it is not possible to independently determine the volume fractions of both magnetic phases and the moments associated with each phase.

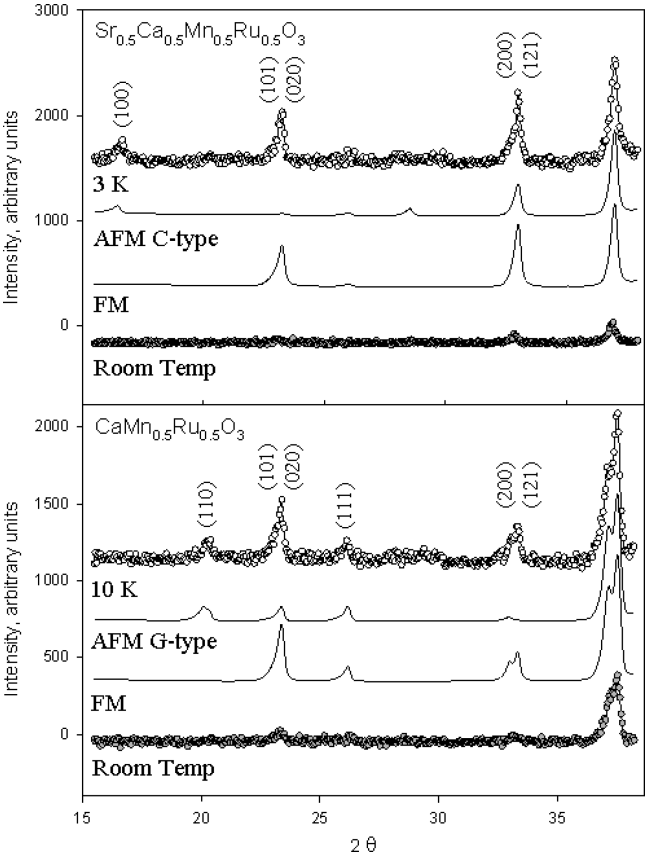

Figure 13. Low-angle region of the NPD data for $Sr_{0.5}Ca_{0.5}Mn_{0.5}Ru_{0.5}O_3$ (top) and $CaMn_{0.5}Ru_{0.5}O_3$ (bottom). The calculated patterns that result from attempts to model the data using only ferromagnetic (FM) or antiferromagnetic (AFM) structures are shown in the middle.

However, we can obtain reasonable estimates of these quantities by making some reasonable assumptions.

First, we assume that the entire sample is magnetically ordered, either ferromagnetically (ferrimagnetically) or antiferromagnetically. Second, we assume that the average moment in the antiferromagnetic structure is 2.1 μ_B per transition metal site. This value is chosen because it is equal to the moment observed for $SrMn_{0.5}Ru_{0.5}O_3$, where homogeneous antiferromagnetic ordering is observed.[11] These two assumptions allow us to refine the volume fractions of the two magnetic phases. Finally, we come to the question of the size of the magnetic moment in the ferromagnetic phase. As discussed in the Introduction, magnetic Compton scattering as well as magnetic circular dichroism measurements indicate that the Mn and Ru moments are aligned antiparallel.[14,16,17] This hypothesis is further supported by the bulk magnetic measurements. However, because the Mn and Ru ions are not chemically ordered, the neutron diffraction measurements are only sensitive to the average scattering power per transition metal site. For manganese we assume 1 μ_B per unpaired electron and assign the number of unpaired electrons based on the XANES estimate of the Mn^{3+}/Mn^{4+} ratio. The ruthenium moment is then set antiparallel and refined.

Using these assumptions, we estimate that 93% of the $CaMn_{0.5}Ru_{0.5}O_3$ sample orders ferrimagnetically, with a moment parallel to the *c*-axis, while 6% orders antiferromagnetically with the G-type structure and a moment parallel to the *b*-axis. If the Mn moment is constrained to a value of 3.33 μ_B per Mn ion, the Ru moment refines to −1.14(7) μ_B per Ru ion. This value is in good agreement with the value of 1.10 μ_B per Ru ion seen in $SrRuO_3$. Furthermore, these values are in reasonably good agreement with the atom specific estimates obtained from magnetic Compton scattering; 3.00 μ_B per Mn and −1.26 μ_B per Ru by Mizusaki et al.,[17] 3.24 μ_B per Mn and −1.42 μ_B per Ru by Taniguchi et al.[14] Finally, we note that the average moment is 1/2(3.33 + 1.14) = 2.2 μ_B per site, which is close to our assumption of 2.1 μ_B per site for the AFM phase.

The $Sr_{0.5}Ca_{0.5}Mn_{0.5}Ru_{0.5}O_3$ sample contains 94% of the ferrimagnetic phase and 6% of the AFM C-type phase. Setting the Mn moment to 3.45 μ_B per Mn ion leads to a refined Ru moment of −1.04(9) μ_B per Ru ion. Because of the pseudocubic nature of the data, we were not able to determine the direction of magnetic moment for either phase.

4. Discussion

A phase diagram for the $Sr_{1-x}Ca_xMn_{0.5}Ru_{0.5}O_3$ system is shown in Figure 14. The most striking feature is a crossover from a tetragonal antiferromagnetic state to an orthorhombic ferrimagnetic state as the calcium content increases. The large tetragonal distortion of the antiferromagnetic Sr-rich samples is a clear sign that antiferromagnetism is closely linked to orbital order. Therefore, understanding the loss of orbital order as Ca^{2+} substitutes for Sr^{2+} is the key to understanding the magnetic behavior. Among the factors that can influence the orbital ordering, the Mn oxidation state is perhaps the most important. Therefore, we begin the discussion with a closer look at the oxidation states of the transition metal ions.

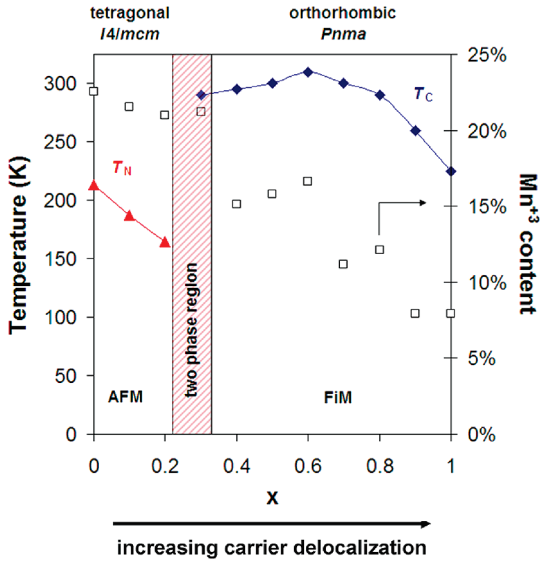

Figure 14. The $Sr_{1-x}Ca_xMn_{0.5}Ru_{0.5}O_3$ phase diagram. The squares show the estimated fraction of octahedral sites that are occupied by Mn^{3+}. This number was calculated by subtracting the Ru oxidation state, as estimated from the XANES spectra, from 8 (the sum of Mn + Ru oxidation states will be equal to 8 assuming no oxygen vacancies). The triangles and diamonds show the Néel and Curie temperatures, respectively.

The Ru L-edge and Mn K-edge XANES data confirm the presence of mixed valency across the entire $Sr_{1-x}Ca_xMn_{0.5}Ru_{0.5}O_3$ series. Quantitative interpretation of the XANES spectra for $SrMn_{0.5}Ru_{0.5}O_3$ gives average oxidation states that lie close to $Mn^{3.5+}$ and $Ru^{4.5+}$. That result coupled with the activated conductivity of this sample suggests that Mn^{3+}, Mn^{4+}, Ru^{4+}, and Ru^{5+} are present in approximately equal concentrations at any given instant. It is interesting to note that in the manganite perovskites C-type antiferromagnetism occurs for Mn^{3+} contents ranging from 37% in $Sr_{0.63}Sm_{0.37}MnO_3$ [41,42] to 20% in $Ca_{0.80}La_{0.20}MnO_3$ [43], 18% in $Ca_{0.82}Bi_{0.18}MnO_3$ [44], and 15% in $Ca_{0.85}Sm_{0.15}MnO_3$.[42] Our estimate of ~23% Mn^{3+} in $SrMn_{0.5}Ru_{0.5}O_3$ (see Figure 14) is near the middle of this range. The strong correlation between orbital and magnetic order and the parallel with the $R_{1-x}Ca_xMnO_3$ perovskites suggests that antiferromagnetism in the Sr-rich samples is stabilized by superexchange interactions, with the orientation of the half-filled Mn e_g orbitals playing a key role.

Although the XANES data do not indicate an abrupt change in valence across the $Sr_{1-x}Ca_xMn_{0.5}Ru_{0.5}O_3$ series (see Figure 14), the Ru L-edge and Mn K-edge XANES

(41) Kurbakov, A. I. *Phys. Solid State* **2009**, *51*, 1210.
(42) Martin, C.; Maignan, A.; Hervieu, M.; Raveau, B. *Phys. Rev. B* **1999**, *60*, 12191.
(43) Wollan, E. O.; Koehler, W. C. *Phys. Rev.* **1955**, *100*, 545.
(44) Santhosh, P. N.; Goldberger, J.; Woodward, P. M.; Vogt, T.; Lee, W. P.; Epstein, A. J. *Phys. Rev. B* **2000**, *62*, 14928.
(45) Hinatsu, Y.; Izumiyama, Y.; Doi, Y.; Alemi, A.; Wakeshima, M.; Nakamura, A.; Morii, Y. *J. Solid State Chem.* **2004**, *177*, 38.
(46) Fu, W. T.; Ijdo, D. J. W. *Solid State Commun.* **2005**, *13*, 456.
(47) Bushmeleva, S. N.; Pomjakushin, V. Yu.; Pomjakushina, E. V.; Sheptyakov, D. V.; Balagurov, A. M. *J. Magn. Magn. Mater.* **2006**, *305*, 491.
(48) Cheah, M.; Saines, P. J.; Kennedy, B. J. *J. Solid State Chem.* **2006**, *179*, 1775.

Table 4. Mn−O and Ru−O Bond Distances in Representative Perovskites; Bond Distances Originate from Samples at Room Temperature unless Otherwise Noted

compd	space group	Ru/Mn−O distance (Å)	ref	compd	space group	Ru/Mn−O distance (Å)	ref
$Ba_2HoRu^{+5}O_6$	*Fm3m*	6 × 1.955	45	$SrMn_{0.5}Ru_{0.5}O_3$ (298 K)	*I*4/*mcm*	4 × 1.947 2 × 1.983 **1.959 (Avg)**	11
$Ba_2NdRu^{+5}O_6$	*Fm3m*	6 × 1.955	46	$SrMn_{0.5}Ru_{0.5}O_3$ (20 K)	*I*4/*mcm*	4 × 1.942 2 × 2.005 **1.963 (*Avg*)**	11
$SrRu^{+4}O_3$	*Pnma*	2 × 1.984 2 × 1.984 2 × 1.988 **1.985 (*Avg*)**	47	$Sr_{0.5}Ca_{0.5}Mn_{0.5}Ru_{0.5}O_3$ (298 K)	*Pnma*	2 × 1.939(5) 2 × 1.979(5) 2 × 1.941(1) **1.953 (*Avg*)**	this work
$CaMn^{+4}O_3$	*Pnma*	2 × 1.897 2 × 1.898 2 × 1.907 **1.901 (*Avg*)**	31	$Sr_{0.5}Ca_{0.5}Mn_{0.5}Ru_{0.5}O_3$ (3 K)	*Pnma*	2 × 1.934(4) 2 × 1.975(4) 2 × 1.956(1) **1.955 (*Avg*)**	this work
$LaMn^{+3}O_3$	*Pnma*	2 × 1.903 2 × 2.177 2 × 1.969 **2.016 (*Avg*)**	2	$CaMn_{0.5}Ru_{0.5}O_3$ (298 K)	*Pnma*	2 × 1.956(2) 2 × 1.957(2) 2 × 1.9427(2) **1.952 (Avg)**	this work
$Sr_2Mn^{3+}SbO_6$	*I*4/*m*	4 × 1.938 2 × 2.098 **1.991 (Avg)**	48	$CaMn_{0.5}Ru_{0.5}O_3$ (10 K)	*Pnma*	2 × 1.950(1) 2 × 1.956(1) 2 × 1.9422(5) **1.949 (Avg)**	this work

data both suggest a significant shift of the $Mn^{3+} + Ru^{5+} \leftrightarrow Mn^{4+} + Ru^{4+}$ equilibrium to the right as x increases. As the Mn^{3+} ions become more dilute, it is not surprising to see a loss of orbital order, which destabilizes the C-type antiferromagnetic state and leads to the emergence of the ferrimagnetic state.

The bond distances extracted from neutron powder diffraction measurements provide an independent check on the valence states of manganese and ruthenium. Unfortunately the lack of Mn/Ru order complicates the analysis. Nonetheless, the average bond distances contain useful information about the predominant oxidation states. Table 4 lists the transition metal−oxygen bond distances for $SrMn_{0.5}Ru_{0.5}O_3$, $Sr_{0.5}Ca_{0.5}Mn_{0.5}Ru_{0.5}O_3$, and $CaMn_{0.5}Ru_{0.5}O_3$ together with a number of perovskites containing manganese and ruthenium for comparison. The expected metal−oxygen distances are 1.901 Å for Mn^{4+}−O, 2.016 Å for Mn^{3+}−O, 1.985 Å for Ru^{4+}−O, and 1.955 Å for Ru^{5+}−O. Because the difference in size between Mn^{3+} and Mn^{4+} is larger than between Ru^{5+} and Ru^{4+}, the average Mn/Ru−O distance is sensitive to the extent of electron transfer between Mn and Ru. The expected average distance is 1.99 Å for the Mn^{3+}/Ru^{5+} redox couple versus 1.94 Å for Mn^{4+}/Ru^{4+} redox couple.

The observed distances for the $x = 0$, 0.5, and 1.0 compositions fall at values that are intermediate between either extreme, supporting the assertion that a $Mn^{3+} + Ru^{5+} \leftrightarrow Mn^{4+} + Ru^{4+}$ valence degeneracy is in fact an accurate description. Furthermore, there is a small but statistically significant decrease in the average bond distance as the calcium content increases, suggesting a shift toward the Mn^{4+}/Ru^{4+} redox pair. Using the values for $CaMnO_3$, $LaMnO_3$, $SrRuO_3$, and Ba_2NdRuO_6 as standard bond distances for each of the integer oxidation states, it is possible to make a semiquantitative estimate of the oxidation states from the average bond distances of the $Sr_{1-x}Ca_xMn_{0.5}Ru_{0.5}O_3$ compounds. The results are given in Table 5. There is good agreement between the bond distance estimate and the XANES estimate.

Table 5. Mn and Ru Valences As Estimated from (a) the Average Mn/Ru−O Distances Obtained at Low Temperature (left) and (b) the Ru L_3 and Mn K-Edge XANES Spectra (right)

	bond distance estimate		XANES estimate	
compd	Mn valence	Ru valence	Mn valence	Ru valence
$SrMn_{0.5}Ru_{0.5}O_3$	3.53	4.47	3.44	4.45
$Sr_{0.5}Ca_{0.5}Mn_{0.5}Ru_{0.5}O_3$	3.72	4.28		4.32
$CaMn_{0.5}Ru_{0.5}O_3$	3.86	4.14	3.65	4.16

Given the fact that Sr^{2+} and Ca^{2+} are isovalent it is not obvious why the Mn/Ru valence degeneracy should shift toward Mn^{4+}/Ru^{4+} as the calcium content increases. While it is not possible to definitively answer this question, an important clue comes from studies of the interplay between octahedral tilting and cooperative Jahn−Teller distortions in ordered perovskites. It has been documented that orbital ordering involving occupied d_{z^2} orbitals all pointing in the same direction (the same type of orbital order that leads to C-type antiferromagnetism) is destabilized by $a^-b^+a^-$ octahedral tilting.[49] Therefore, as calcium replaces strontium and the tolerance factor decreases, eventually a transition from a tetragonal structure with $a^0a^0c^-$ tilting to an orthorhombic structure with $a^-b^+a^-$ tilting occurs. The extra octahedral tilting disrupts the orbital ordering. In many compounds, the local Jahn−Teller distortions of the Mn^{3+} octahedra would not disappear, they would simply become increasingly uncorrelated. However, in the $Sr_{1-x}Ca_xMn_{0.5}Ru_{0.5}O_3$ series there is another option. The energy levels of the Mn and Ru d-orbitals are placed such that electron density can be transferred from Mn to Ru, which reduces the concentration of Mn^{3+} and lessens bond strains arising from local, noncooperative Jahn−Teller distortions.

(49) Lufaso, M. W.; Woodward, P. M. *Acta Crys. B* **2004**, *60*, 10.

The link between octahedral tilting and orbital ordering plays not only an indirect role of shifting the manganese valence, it likely plays a direct role in the crossover from antiferromagnetism to ferrimagnetism. After all, the ruthenium, and hence manganese, valence does not change as abruptly as the magnetism does. Furthermore, there is some evidence in the bond distances of the $Sr_{0.5}Ca_{0.5}Mn_{0.5}Ru_{0.5}O_3$ sample for partial *ac*-plane orbital ordering, as seen in $LaMnO_3$ [3]. It has been shown that $LaMnO_3$-type orbital ordering involving Mn $3d_{3x^2-r^2}$ and Mn $3d_{3z^2-r^2}$ orbitals becomes more pronounced if anything as the octahedral tilting increases.[49] Therefore, it is not unreasonable that a change in the preferred type of orbital order can be triggered by a change in the tilt system. An interesting parallel comes from the studies of $LaMn_{0.5}Ga_{0.5}O_3$ and $NdMn_{0.5}Ga_{0.5}O_3$ by Cussen et al.[50] $LaMn_{0.5}Ga_{0.5}O_3$ is a ferromagnetic insulator (T_C = 70 K) that does not exhibit a CJTD, implying a nearly complete lack of orbital order. Substitution of the smaller Nd^{3+} ion decreases the tolerance factor which triggers a large CJTD, which in turn leads to a significant antiferromagnetic canting of the magnetic structure (T_C = 40 K).

Arguably the most interesting aspect of the work is the observation of ferrimagnetic behavior with T_C values approaching room temperature in samples containing a disordered arrangement of two different transition metal ions. The ferrimagnetic alignment of Mn and Ru is reminiscent of the behavior of Sr_2FeMoO_6, where the Fe moments are localized and ferromagnetically coupled, while the Mo-based electron is delocalized and aligned antiparallel to the localized electrons. The net result is a half-metallic ferrimagnet with a T_C of 410 K.[51] However, unlike $CaMn_{0.5}Ru_{0.5}O_3$, the magnetism of Sr_2FeMoO_6 is very sensitive to antisite disorder, due to strong antiferromagnetic Fe−O−Fe superexchange coupling. The high T_C ferrimagnetic state is lost if the Fe/Mo ions become completely disordered. Complete disorder is observed in $SrFe_{0.5}Ru_{0.5}O_3$, where spin glass behavior results from the disorder.[52]

The comparison with the Fe-containing perovskites raises an interesting question. Why don't Ca-rich samples, which lack both chemical and orbital order, exhibit spin/cluster glass behavior? An important difference between iron and manganese is the flexibility of the $t_{2g}^3e_g^1$ electron configuration of Mn^{3+}. If the e_g electron is localized, it can stabilize ferromagnetic superexchange coupling with two out of its six neighbors. It could also partially delocalize so that it is shared by two or more Mn centers to form a ferromagnetically coupled Zener polaron. These possibilities provide an avenue whereby neighboring Mn ions can couple ferromagnetically to each other, retaining the net ferrimagnetism. No such mechanisms exist in the Fe-containing double perovskites.

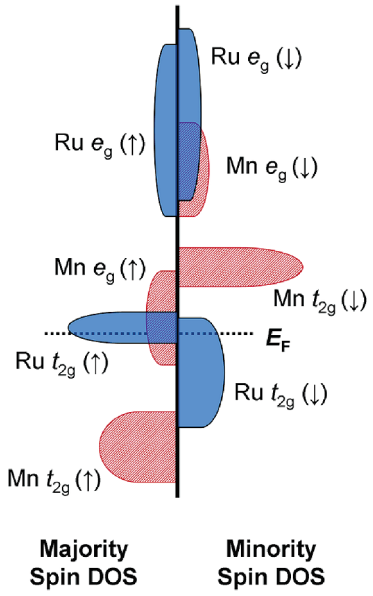

Figure 15. Schematic spin polarized band structure for ferrimagnetic $Sr_{1-x}Ca_xMn_{0.5}Ru_{0.5}O_3$ samples. The bands where the Mn character is dominant are shown in red, whereas the bands where the Ru character is dominant are shown in blue.

The picture that emerges for the ferrimagnetic $Sr_{1-x}Ca_xMn_{0.5}Ru_{0.5}O_3$ samples is one where Mn t_{2g} electrons are localized and ferromagnetically aligned with each other. We will arbitrarily label these electrons as spin up. The Ru t_{2g} orbitals form a band where the spin down states are energetically favored through hybridization with the spin down Mn t_{2g} orbitals, but are not completely offset from the up spin Ru t_{2g} orbitals (see Figure 15). This is analogous to Sarma's double perovskite double exchange model for ferrimagnetism in Sr_2FeMoO_6.[53] The up spin Ru t_{2g} band is quite narrow, as these electrons cannot move through the Mn sites because of the Pauli exclusion principle. The incomplete polarization of the Ru t_{2g} bands helps to explain why the Ru moment is reduced from the 2−3 μ_B per Ru ion that would be expected in the localized picture, to the value of ~1.1 μ_B per Ru ion estimated from the neutron diffraction analysis.

A key difference between $CaMn_{0.5}Ru_{0.5}O_3$ and Sr_2FeMoO_6 is the lack of cation order in the former compound. In Sr_2FeMoO_6, this disorder destabilizes the ferrimagnetic arrangement. In $CaMn_{0.5}Ru_{0.5}O_3$, we propose that the Mn e_g electrons are delocalized between pairs or small clusters of neighboring Mn atoms, to form ferromagnetically coupled Zener polarons. In this way, the Mn e_g electrons can compensate for "mistakes" that result from disorder thereby inhibiting nucleation and growth of antiferromagnetic clusters. If this explanation is correct, the Mn^{3+} concentration should be closely linked to the magnetic behavior. This may help to explain why T_C is highest for intermediate values of x, dropping from 290 K for $Sr_{0.5}Ca_{0.5}Mn_{0.5}Ru_{0.5}O_3$ to 230 K for $CaMn_{0.5}Ru_{0.5}O_3$.

(50) Cussen, E. J.; Rosseinsky, M. J.; Battle, P. D.; Burley, J. C.; Spring, L. E.; Vente, J. F.; Blundell, S. J.; Coldea, I.; Amalia, I.; Singleton, J. *J. Am. Chem. Soc.* **2001**, *123*, 1111.
(51) Kobayashi, K.-I.; Kimura, T.; Sawada, H.; Terakura, K.; Tokura, Y. *Nature* **1998**, *395*, 677.
(52) Battle, P. D.; Gibb, T. C.; Jones, C. W.; Studer, F. *J. Solid State Chem.* **1989**, *78*, 281.
(53) Sarma, D. D.; Mahadevan, P.; Saha-Dasgupta, T.; Ray, S.; Kumar, A. *Phys. Rev. Lett.* **2000**, *85*, 2549.

As shown in Figure 13, the XANES analysis suggests a correlation between the Mn oxidation state and the T_C.

By the time we reach $CaMn_{0.5}Ru_{0.5}O_3$, the Mn^{3+} concentration is no longer sufficient to completely suppress nucleation of antiferromagnetic clusters, leading to the phase separation observed in the susceptibility and neutron measurements. The antiferromagnetic regions presumably nucleate in clusters rich in Mn^{4+}. The T_C (~95 K) and structure type (G-type) are fairly similar to pure $CaMnO_3$. It is important to note that the antiferromagnetic regions seen in $Sr_{0.5}Ca_{0.5}Mn_{0.5}Ru_{0.5}O_3$ are C-type rather than G-type. The phase separation in the $x = 0.5$ sample appears to be driven by a different mechanism, one where short-range orbital ordering stabilizes regions that retain the C-type antiferromagnetism characteristic of Sr-rich samples.

5. Conclusions

A $Mn^{3+} + Ru^{5+} \leftrightarrow Mn^{4+} + Ru^{4+}$ valence degeneracy exists for the entire $Sr_{1-x}Ca_xMn_{0.5}Ru_{0.5}O_3$ perovskite system. On the Sr-rich end ($x \leq 0.2$) the average oxidation states are close to $Mn^{+3.5}$ and $Ru^{+4.5}$. The presence of ~23% Mn^{3+} and the relatively large tolerance factor ($\tau \approx 0.99$) favor parallel ordering of the Mn $3d_{z^2}$ orbitals. This pattern of orbital ordering leads to a tetragonally distorted unit cell with C-type antiferromagnetic ordering, that is stabilized through superexchange interactions. Replacing strontium with the smaller calcium lowers the tolerance factor driving additional rotations of the octahedra, changing the structure from tetragonal ($a^0a^0c^-$ tilting) to orthorhombic ($a^-b^+a^-$ tilting) for $x > 0.2$. The tetragonal to orthorhombic transition is accompanied by (a) a loss (or at least significant reduction) in orbital order, (b) a shift in the valence degeneracy toward $Mn^{4+} + Ru^{4+}$, and (c) a crossover from antiferromagnetism to ferrimagnetism. Further increases in the calcium content result in more pronounced octahedral tilting, further transfer of electron density from Mn to Ru, and eventually a decrease in T_C. The observation of ferrimagnetism with a T_C that exceeds room temperature is rather surprising given the complete lack of Mn/Ru order. A model is proposed whereby the ferrimagnetic state is stabilized by two different mechanisms. Double perovskite double exchange is responsible for the ferrimagnetic alignment of Mn and Ru. In this model the electrons in the minority (down) spin Ru t_{2g} orbitals are itinerant and responsible for the relatively high conductivity seen for Ca-rich samples. Conventional double exchange between neighboring Mn ions (forming Zener polarons) is responsible for maintaining the parallel alignment of the Mn ions in the presence of chemical disorder. For the most Ca-rich samples, $x > 0.8$, the Mn^{3+} ions become too dilute to completely prevent nucleation of antiferromagnetic (G-type) regions, leading to a relatively small degree of phase separation.

Acknowledgment. We thank Ray Withers and Michelle Dolgos for collecting electron diffraction analysis, as well as Adam Hauser, Jeremy Lucy, and Fengyuan Yang for assistance with the VSM measurements and Rene Macquart for the AC measurements. R.A.R., H.L.C., and P.M.W. acknowledge the Center for Emergent Materials at the Ohio State University, an NSF MRSEC (Award DMR-0820414), for providing funding for this research. B.J.K. acknowledges the support of the Australian Research Council. The synchrotron measurements were supported by the Australian Synchrotron Research Program under the Major National Research Facilities Program.